PHOTONICS Research

Orbital angular momentum mode logical operation using optical diffractive neural network

Peipei Wang,[1] Wenjie Xiong,[1] Zebin Huang,[1] Yanliang He,[1] Zhiqiang Xie,[1] Junmin Liu,[2] Huapeng Ye,[3] Ying Li,[1] Dianyuan Fan,[1] and Shuqing Chen[1,*]

[1]International Collaborative Laboratory of 2D Materials for Optoelectronics Science and Technology, Institute of Microscale Optoelectronics, Shenzhen University, Shenzhen 518060, China
[2]College of New Materials and New Energies, Shenzhen Technology University, Shenzhen 518118, China
[3]Guangdong Provincial Key Laboratory of Optical Information Materials and Technology and Institute of Electronic Paper Displays, South China Academy of Advanced Optoelectronics, South China Normal University, Guangzhou 510006, China
*Corresponding author: shuqingchen@szu.edu.cn

Received 1 June 2021; revised 12 August 2021; accepted 20 August 2021; posted 24 August 2021 (Doc. ID 432919); published 30 September 2021

Optical logical operations demonstrate the key role of optical digital computing, which can perform general-purpose calculations and possess fast processing speed, low crosstalk, and high throughput. The logic states usually refer to linear momentums that are distinguished by intensity distributions, which blur the discrimination boundary and limit its sustainable applications. Here, we introduce orbital angular momentum (OAM) mode logical operations performed by optical diffractive neural networks (ODNNs). Using the OAM mode as a logic state not only can improve the parallel processing ability but also enhance the logic distinction and robustness of logical gates owing to the mode infinity and orthogonality. ODNN combining scalar diffraction theory and deep learning technology is designed to independently manipulate the mode and spatial position of multiple OAM modes, which allows for complex multilight modulation functions to respond to logic inputs. We show that few-layer ODNNs successfully implement the logical operations of AND, OR, NOT, NAND, and NOR in simulations. The logic units of XNOR and XOR are obtained by cascading the basic logical gates of AND, OR, and NOT, which can further constitute logical half-adder gates. Our demonstrations may provide a new avenue for optical logical operations and are expected to promote the practical application of optical digital computing.

https://doi.org/10.1364/PRJ.432919

1. INTRODUCTION

Optical computing, which performs numerical computations on one-dimensional or multidimensional data with light wave radiation [1,2], exhibits ultrafast computing speed and parallel computing capability owing to the light-speed propagation and superposition characteristics of photons [3], and has attracted extensive attention in augmented reality, autonomous driving [4], pattern recognition [5], and more. Optical analog calculations, combined with linear or nonlinear optical elements to perform continuous function conversions [6], are usually used for optical imaging [7,8], such as convolution and correlation, which are bound by limited flexibility and high noise susceptibility [2]. The second class of optical computing is optical digital calculation, which is implemented by the logical gates formed by light field propagation and optical modulation, which can perform general-purpose calculations and avoid noise accumulation [9]. However, logic states "1" and "0" are often expressed by the strength of amplitude, where the poor anti-interference ability, low contrast, and difficulty in high-order modulation seriously hinder its development. One approach to improve the performance of logic is to find a suitable physical dimension with more orthogonal bases to express logic variables. Orbital angular momentum (OAM) modes [10,11] carried by vortex beams have been widely employed in various fields [12–24] for their mode infinity and orthogonality. The obvious mode distinction, discrimination robustness, and sufficient modulation freedom endow the OAM with a controllable physical dimension of logic states to improve computing performance and applicability. How the multiple light fields are independently controlled with diversified input positions and phases, however, remains elusive in OAM logic, which ensures responses to input logic states.

Optical logical operations mostly rely on linear interference [25–28] and nonlinear effects [29,30]. By modulating the basic physical properties (including phase, amplitude, and polarization) of incident light using interference theory or optical nonlinear effects, basic OR and NOT gates were obtained according to the interference distribution or strength of the

output intensity [25,31]. These methods modulate intensity distributions, and the structural integrity of the original light fields is usually destroyed, which is difficult to maintain and sustainably transmit the spatial spiral phase front of vortex beams. The multiplane diffractive structure shows a complex modulation ability in independently modulating multiple OAM modes to expand the control dimension and depth of light fields via multiple wavefront modulation [32,33]. To obtain the diffractive structures, the wavefront matching algorithm [34] is typically used to iteratively calculate the phase distribution of the light field superimposed by the forward and backward propagations at each diffraction screen, and mode conversion among three OAM modes was realized [35]. This algorithm lacks an effective optimization function, and the phases are optimized only by calculating the conjugate product of the superimposed fields with a simple matching formula, causing the iterative process to easily fall into the local optimal dilemma and leading to a low modulation accuracy. Recently, optical diffractive neural networks (ODNNs) [36–40] compatible with deep learning and light field modulation capabilities have been proposed to modulate the OAM mode [41] and exhibit excellent information processing ability. However, its modulation target mainly aims at the mode conversion of a single vortex beam. The construction of OAM logic and the independent modulation of mode and spatial position of multiple modes remain challenges to be explored in optical digital computing.

Using mode infinity and orthogonality, we introduce the OAM logical operations implemented by ODNNs. With a large phase difference in the wavefronts of the OAM modes and the protected structural integrity by controlling the angular momentum, the OAM logical operation can significantly improve the boundary definition, robustness, and computing power of logic gates. The main difficulty in performing OAM logical operations is independently modulating multiple light fields in the spatial position and mode conversion. We design an ODNN-physical model that combines the scalar diffractive theory and deep learning technology to calculate the common multiplane diffractive structure to possess multiple OAM mode responses and modulation capabilities, which is capable of handling binary and multiary OAM logic operations. The ODNN model solves the linear response of multiple light fields by linking multilayer phases and amplitudes, and accurately implements seven basic binary logical operations, AND, OR, NOT, NAND, NOR, XNOR, and XOR gates, and a half-adder in simulations. In addition to not destroying the physical characteristics of input beams and efficiently completing logical operations, this method can be extended to multiary logical operations, providing a potential solution for the practical application of optical digital computing.

2. PRINCIPLES AND RESULTS

A. OAM Mode Logical Operation with ODNN

OAM contributed by the spiral phase factor $\exp(il\theta)$ has mode infinity and orthogonality, where the topological charge l represents the order of the OAM mode, and θ is the azimuth angle [42]. We generated OAM modes using Laguerre-Gaussian beams with a working wavelength of 1550 nm and a waist radius of 2 mm. By virtue of the large phase difference in the wavefronts, the OAM modes are employed as logic states. According to the operation requirements, we select two OAM modes with $l = 1, 2$ to represent logical constants "0" and "1," respectively (OAM modes are uniformly represented by logical constants below).

For binary logical gates, input data mainly include four states, "00," "01," "10," and "11," corresponding to four input light fields permuted and combined by OAM_1 and OAM_2 in logical operations, where the subscript indicates the topological charge value. To differentially control the four light fields, we construct an ODNN model with updatable phase and amplitude parameters to perform OAM logical operations. Figure 1 shows the light field processing schematic diagram of a k-layer ODNN, and the construction principle is described in detail in the "Methods" section. The input data are two OAM modes incident from different spatial positions, and the main task of the ODNN is to perform independent modulation of the input light fields and ensure the transformation satisfies the calculation rule of logical gates. After wavefront modulation of multiple diffraction screens and diffraction transmission, a vortex beam carrying one OAM mode is emitted at the center of the output screen. Similarly, it is expected that the ODNN can synchronously modulate the mode and spatial position of the OAM modes. The exceptional logic NOT gate only requires one input port for two input states "0" and "1," which is different from the working principle of other logical gates; this will be introduced in detail below.

B. OAM Logic AND, OR, NOT, NAND, and NOR Gates

We start with the design of the OAM logic AND gate, and the training dataset of the ODNN, including four light-field pairs, is shown in Fig. 2. The first row displays the intensity distributions of the input beams, and the period from blue to red represents the order of the OAM mode. Using A and B to represent the two logic variables, the values can take any one of the two modes (OAM_1 and OAM_2). The output of the logical operation can be expressed as

$$Y = f(A, B), \tag{1}$$

where f represents the logical operation function. The ideal outputs of the logic AND gate are shown in the second row of Fig. 2, and the logical operations obey the rule of $Y = A \cdot B$.

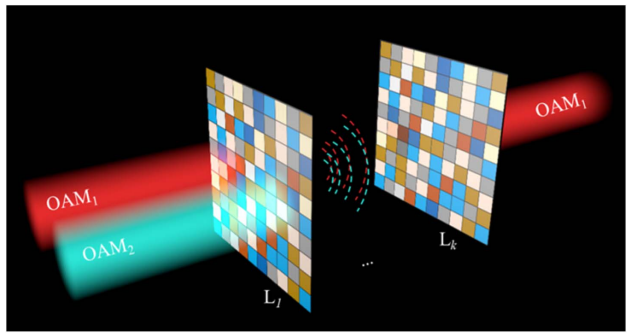

Fig. 1. Schematic of OAM mode logical operation based on ODNN.

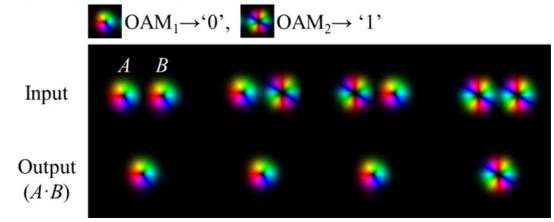

Fig. 2. Training data set of OAM logic AND gate.

By feeding these four data samples to a four-layer ODNN, the loss value is decreased by constantly updating and adjusting the phase and amplitude distributions of diffractive layers, and the graph of the loss function in training is shown in Fig. 3(a). During the iterative process, the loss value drops sharply at the beginning and then stabilizes, which means that the network model converges continuously as the loss function approaches zero. After being trained with 8000 iterations, the ODNN can calculate and match the diffractive structures to independently modulate the four input fields; the training process took approximately 20 min with the graphics processing unit, Intel Core i9-10900k. From the phase and amplitude patterns trained by the ODNN [see Fig. 3(b)], valid information is mainly concentrated in the center, which is caused by the input and output beams that all illuminate the center position. Theoretically, by designing metasurfaces [43–46] according to the modulation structure parameters or loading them on spatial light modulators, the OAM logic AND operation can be implemented experimentally.

Due to the ODNN model being trained by four input states simultaneously, the obtained logic AND gate can accurately response and modulate all these states without changing the diffractive structures. The predicted outputs of the ODNN trained for logic AND operations are displayed in Fig. 4(a), and the inset in the upper left corner of each subfigure is

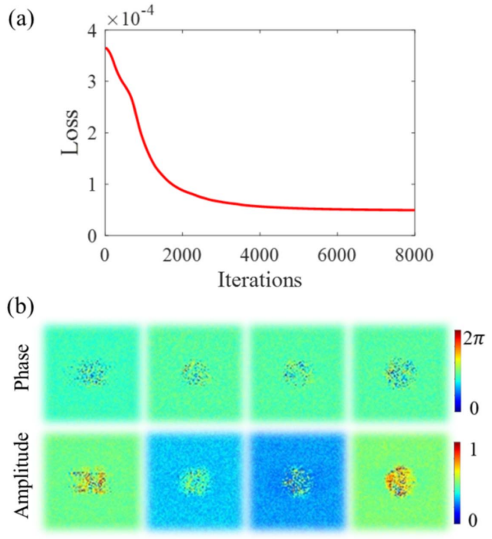

Fig. 3. Training results of ODNN with logic AND operation. (a) Curve of the loss function with the iteration number. (b) Phase and amplitude distributions of diffractive layers.

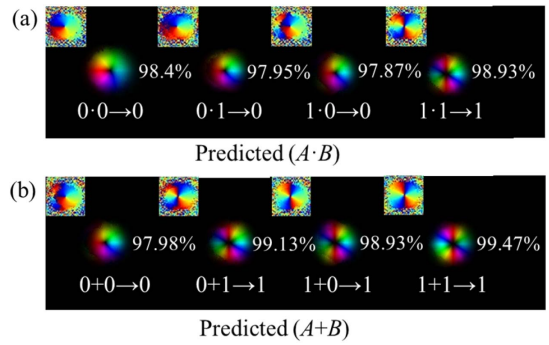

Fig. 4. Modulation results of ODNN with different logical operations. (a) Logic AND gate. (b) Logic OR gate.

the corresponding phase distribution of output. To quantize the goodness of matching between predicted results and ideal outputs, we test the mode purity of predicted outputs, which can be calculated by $p = J_G/J_T$, where J_G is the light energy of the filtered Gaussian beam obtained by degrading the output beam through a conjugate OAM mode, and J_T is the total energy of the output beam. The mode purities are shown in the figures as a percentage to represent the prediction accuracy of the model. These figures show that the obtained light fields on the observation screen have expected OAM modes, which are exactly equal to the output mode orders after logic AND operation, and the mode purities exceed 97%. Next, we train an ODNN with the same input data to implement the logic OR operation, and the output OAM modes must satisfy the function of $Y = A + B$. Figure 4(b) shows the simulated modulation results of the trained ODNN model with $k = 4$, which demonstrates that the ODNN solves the response of the multiplane diffractive device for the four input beams with different modulation requirements. For example, the ODNN accurately completed the logic OR operation of "0 + 1" for the OAM_1 and OAM_2 modes and output OAM_2 with a mode purity of 99.13%.

As a special logical gate, the NOT gate only has two input states, "0" and "1." Therefore, the essence of the logic NOT operation is to exchange the mode between OAM_1 and OAM_2. Figure 5(a) shows a schematic for the NOT operation, where

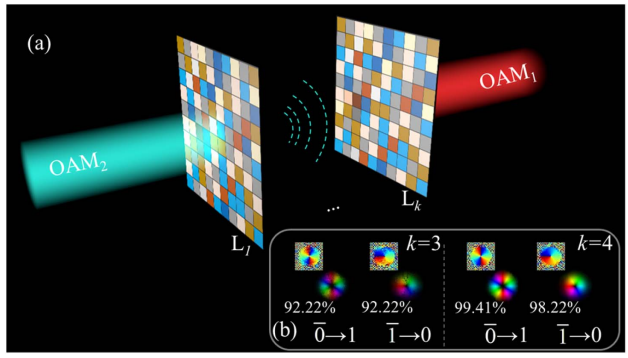

Fig. 5. OAM logic NOT gate based on ODNN. (a) Schematic of the light field modulation by ODNN. (b) Predicted results of ODNNs with different layers.

the single OAM modes occur on the center of the first diffractive layer and continue to transmit along the original path after mode modulation. The input represented by one logic variable A contains two states, which requires only two data pairs in the training set, and the conversion can be expressed by $Y = \bar{A}$. To coaxially and independently modulate these two OAM modes, we constructed ODNNs with different layers to train the NOT gates, and the results are shown in Fig. 5(b). The quality of the output predicted by the three-layer ODNN model was slightly lower than that of the four-layer model. From the brightness of the light fields, the energy utilization rate is decreased because the modulation ability of the three-layer diffractive structure is insufficient to process all information, leading to energy dispersion. Thereby, the mode purities are reduced. However, the phase distributions demonstrate that the mode information has been accurately modulated, and it is sufficient to complete accurate logical operations for the OAM NOT gate.

Furthermore, we train four-layer ODNNs to modulate the OAM modes to implement NAND and NOR operations. After training these four data shown in Fig. 6(a) with multiple iterations, the two ODNNs successfully mapped $Y_{\mathrm{NAND}} = \overline{A \cdot B}$ and $Y_{\mathrm{NOR}} = \overline{A + B}$ between the input and output logic states, respectively. Figure 6(b) shows the modulation results of the NAND and NOR gates. For all input states, the ODNNs can accurately control the OAM mode and spatial position. This indicates that the designed ODNN can be used as a general method to independently modulate multiple light fields, and the network model can complete some mathematical operations, such as the addition and multiplication of the logical states studied above.

C. OAM Logic XNOR and XOR Gates

In addition to the five basic operations of AND, OR, NOT, NAND, and NOR, the logical operations of XNOR and XOR also have important applications in digital computing. For the XNOR operation with the operational rule of $Y = \bar{A}\bar{B} + AB$, we realize it by cascading the AND, OR, and NOT gates, and the schematic diagram is shown in Fig. 7(a). The logic variables A and B are transmitted through a NOT gate, respectively, which are simultaneously modulated by the AND gate to complete the operation $\bar{A} \cdot \bar{B}$, and the output is sent to the OR gate together with the result of the $A \cdot B$ operation implemented by another AND gate to perform the addition operation. Here, we

(a)

A	B	Y_{NAND}	Y_{NOR}
0	0	1	1
0	1	1	0
1	0	1	0
1	1	0	0

(b)

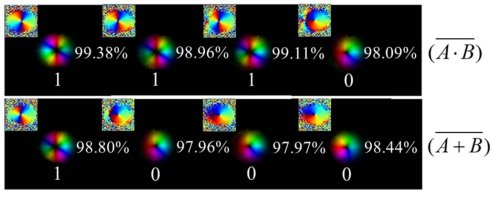

Fig. 6. (a) Operation truth table and (b) prediction outputs by ODNNs for OAM logic NAND and NOR gates.

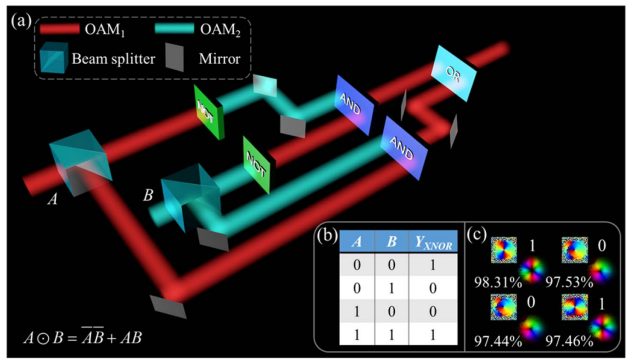

Fig. 7. Logic XNOR gate cascaded by the basic logic AND, OR, and NOT units. (a) System diagram of XNOR operation based on cascaded logical gates. (b) Truth table. (c) Predicted results of logic XNOR operation with four input states of "00," "01," "10," and "11."

used the cascaded multiple ODNN models to construct the XNOR gate. The values of the logic variables are shown in the truth table [see Fig. 7(b)]. For two identical logic states, the ideal output of XNOR is OAM_2; otherwise, it is OAM_1. By inputting these four logic states into the cascaded logic gates, the output response states are obtained, as displayed in Fig. 7(c). It can be observed that the cascaded OAM logical gates accurately completed the logic XNOR operation, and all mode purities exceed 97%. Note that we neglected fabrication errors and reflection loss during the simulation.

For the logic XOR gate, we also constructed it by cascading basic AND, OR, and NOT gates. The designed system is shown in Fig. 8(a). The logic function of $A\bar{B} + \bar{A}B$ can be jointly performed by two AND gates, two NOT gates, and one OR gate. Similarly, we make the logic variables take values from the truth table shown in Fig. 8(b) from top to bottom. The results are presented in Fig. 8(c). These figures show that the phase and intensity distributions of these output light fields conform to expectations, and the mode purities are about 97%, which demonstrates that the OAM logical operations can avoid the destruction of the original light field structures in most traditional optical logics. Theoretically, the proposed OAM logic gates can accurately implement logical operations without

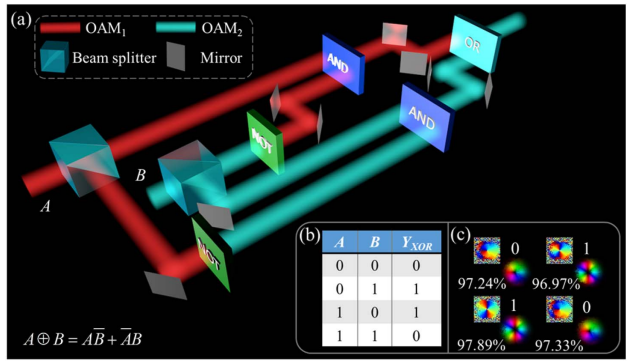

Fig. 8. Schematic illustration of logic XOR operation. (a) System diagram of XOR gate cascaded by logic AND, OR, and NOT gates. (b) Truth table. (c) Phase and intensity distribution of results predicted by the logic XOR gate.

affecting the long-distance transmission of the original optical field signals, which is more suitable for practical optical digital calculations.

There are two main reasons for cascading three basic logic gates to implement XNOR and XOR operations instead of building an ODNN model. First, the calculation is more complicated. The XNOR and XOR operations include three operations simultaneously, namely, multiplication, addition, and inverse, which are difficult for one ODNN. Second, the feature of the data distribution is more hidden. Different from the other five logic operations with a stronger data regularity, where the "0" or "1" appears three times in the ideal outputs of training data, the feature information contained in the training data of the XNOR and XOR operations is fuzzier, making it difficult for the ODNN model to match the modulation relationship between the four data pairs and calculate the structural parameters of the diffractive layers.

D. OAM Half-Adder

To explore the application of OAM logical gates in optical digital computing, we constructed a half-adder by cascading the designed logical gates. Because the half-adder does not need to consider the Carry sent from the low bit, we only calculated the standard sum of two one-bit binary data A and B. According to this principle, we constructed the optical structure of the half-adder, as shown in Fig. 9(a). The half-adder has two output bits, Carry C and sum S, whose response mechanisms are exactly the same as the operation of the AND gate and XOR gate, respectively. Thus, we combine the XOR and AND gates to construct an OAM mode-based optical half-adder [see Fig. 9(a)]. The input logic variables A and B are both divided into two sub-beams with a 50:50 ratio, one of which is incident into the logic XOR gate for standard sum operation, and the other is modulated by the AND gate to calculate the Carry value. The values of the logic variables and ideal output states for the addition of two one-bit binary data are shown in the truth table in Fig. 9(b). These four input states were sequentially input to the constructed half-adder to verify the calculation accuracy. The results in Fig. 9(c) show that the mode

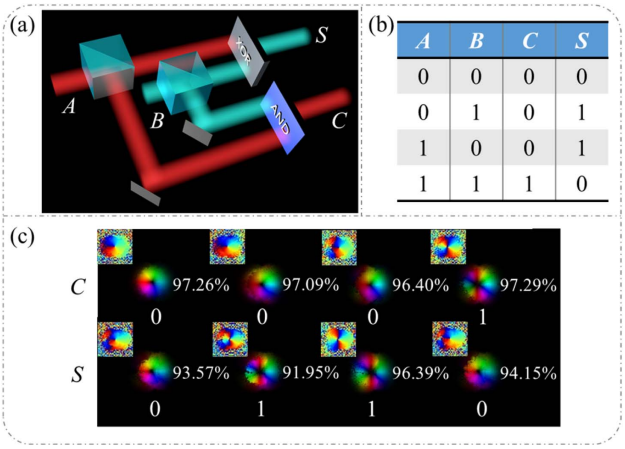

Fig. 9. Schematic illustration of the half-adder based on the OAM mode. C: Carry. S: sum. (a) System diagram of the half-adder cascaded by the XOR and AND gates. (b) Truth table. (c) Results of the addition operation performed by the half-adder.

purities are all greater than 91%, which confirms that the proposed ODNN-based OAM logical gates can be used in optical digital computing. Similarly, it can also be expanded to construct a full adder by considering the Carry from the lower bits by cascading multiple basic logic units, which can realize full addition operations with wider applications.

3. DISCUSSION

Using the OAM mode as a logic state can complete high-accuracy and robustness logical operations, which is mainly attributed to the fact that the mode features among OAM modes are quite different (manifested in phase and intensity distributions), and they can maintain strong mode discrimination even when disturbed. Compared with electrical logic gates, whose transmission rate and computing power are limited by dilemma of Moore's law and the tidal load effect of the von Neumann architecture, and the voltage level is used as the logic state; the ODNN-based OAM logics not only have ultrafast computing speed and parallel computing capability, but also greatly improve the expression ability of logic states and have strong fault tolerance. These advantages are more evident in the compound logic units such as XNOR and XOR, because the electrical logic gates are susceptible to voltage fluctuation, temperature, and current mutual inductance. Compared with traditional optical logic gates that use intensity as logic states, OAM logic can manipulate the independent physical dimension of the OAM mode to complete logical operations while maintaining the structural integrity of light fields, which endows the constructed basic logic gates with the ability to be combined into compound logical arithmetic units. For the ODNN, it is used to solve the key problem of independent modulation of multiple light fields, including calculating the structural parameters of diffractive layers. The excellent information processing capability enables the OAM logic to take any desired OAM mode as a logic state and realize high-ary logic operations, which are difficult for traditional electrical and optical logics. In addition to the above-mentioned seven logic gates and adder, other complex logic devices, such as all-optical encoders, decoders, and data selector, are expected to be realized. More interestingly, the OAM mode can be converted into current signals through photodetectors [47], which allows the OAM logic gates to be combined with the circuit system to obtain large-scale optical-electric fusion logic systems.

For the experimental realization of OAM logical operations, the diffractive layers in OAM logic can be achieved by spatial light modulators, metasurfaces, and three-dimensional printing [48,49], and the constructed ODNN model can be used as an inverse design algorithm to design modulation devices. In the experiment, it is usually necessary to detect the output mode of OAM logics and distinguish the output states, which can be accomplished by back conversion, diffraction, and interference methods [50–53]. In addition, these methods can combine with deep learning technologies to improve the detection accuracy, range, and anti-interference ability [54–56].

Considering that the practical inputs are difficult to perfectly match the inputs in simulations, we further explore the robustness of the constructed logic gates. Since the beam radius in experiment has a certain uncertainty, we first explore

Table 1. Test Results of Four Input States with Different Waist Radii

	Original Model				Model Trained with Different Waists			
w_0	00	01	10	11	00	01	10	11
1.5	75.27%	47.81%	61.45%	40.52%	94.42%	93.26%	92.74%	92.46%
1.6	81.73%	55.72%	69.02%	47.82%	95.84%	95.13%	94.74%	95.03%
1.7	87.62%	65.51%	76.70%	57.13%	96.75%	96.17%	95.89%	96.33%
1.8	92.75%	77.90%	84.82%	70.47%	97.37%	96.82%	96.62%	97.06%
1.9	96.63%	91.28%	93.04%	88.34%	97.80%	97.26%	97.13%	97.58%
2.0	98.40%	97.95%	97.87%	98.93%	98.10%	97.60%	97.52%	98.03%
2.1	96.98%	92.23%	90.20%	89.41%	98.30%	97.86%	97.80%	98.40%
2.2	91.86%	81.08%	68.89%	74.59%	98.41%	98.01%	97.96%	98.57%
2.3	83.81%	71.62%	50.74%	64.45%	98.45%	97.99%	97.91%	98.41%
2.4	74.73%	65.13%	41.93%	58.42%	98.40%	97.72%	97.53%	97.79%
2.5	66.41%	60.87%	38.44%	54.77%	98.27%	97.11%	96.67%	96.62%

the influence of the waist radius w_0 on the performance of the trained model. For the logic AND gate trained with $w_0 = 2$ mm, we set 1.5 mm as an initial value and 0.1 mm as the interval to increase the waist radius (that is, 11 different waist radii), and 44 test data are obtained and fed to the model. The results in Table 1 show that for input states with large changes in radius, the output mode purities are significantly reduced, which is mainly because the matching relationships between the modulation information and the input signals are destroyed. To enhance its adaptability, we introduce the waist radius into the training data. Under the same network structure, after trained by these 44 data, the 4-layer ODNN-based logic AND gate can accurately respond to all inputs with different waist radii. And for the data with $w_0 = 2.6$ mm, 2.7 mm, and 2.8 mm that are not included in the training set, the mode purities of the outputs are (98.04%, 96.10%, 95.20%, 94.87%), (97.68%, 94.64%, 93.05%, 92.56%), and (97.18%, 92.74%, 90.22%, 89.76%), all values exceeding 89%, which means that the robustness of the trained model has been greatly improved. During training, the number of training iterations was reduced to 3000 to save training time. At the same time, we test the robustness of the trained AND gate to the rotation of the phase distributions of input OAM modes. We rotate the phase distributions of the four inputs from 0° with an interval of 30°, and the results demonstrate that the mode purities of the four outputs are 98.40%, 97.95%, 97.87%, and 98.15%, respectively, which are consistent with the output results without rotation. As a demonstration, we present the outputs of the AND gate for the four input states with rotation angles of 90° and 180° in Fig. 10. From the figure, all input states are accurately responded and modulated by the model, and the output OAM modes have the same phase rotation, indicating that the constructed logic gate is insensitive to phase rotation. In addition, since OAM mode is easily distorted by transmission disturbance, we introduce atmospheric turbulence to study the modulation ability of the models for the inputs with a certain error. In simulations, the Hill-Andrew model [57] was used to generate turbulence phases, where the inner and outer scales of atmospheric turbulence are 0.2 mm and 50 m, the turbulence equal propagation distance z is 10 m, which is a factor affecting disturbance degree, and the practical propagation distance in free space is 20 cm. Table 2 shows the test results of the trained AND gate for four input signals with different turbulence strengths C_n^2. From the table, the mode purities of outputs remain above 80% as the turbulence strength increases from 1×10^{-16} to 1×10^{-15} $m^{-2/3}$, indicating that the model has a certain robustness under weak disturbances. With the further increase of C_n^2, the modulation performance of the ODNN drops sharply due to the input signals are severely distorted. This problem can be alleviated by introducing a certain error into the training data to improve the sample diversity.

Furthermore, we investigate higher-ary logic. We train a 5-layer ODNN model with a balanced ternary logic AND operation function, and the operating rules are shown in the truth table [see Fig. 11(a)]. The logic states "−1," "0," and "1" represent the constants "false," "unknown," and "true," respectively, which are closer to the mode of human brains. Logic variables A and B can take any value of the three logic states and provide nine training samples for the ODNN. Similarly, we selected OAM modes with topological charges of 1, 2, and 3 to represent logic states "−1," "0," and "1." After being

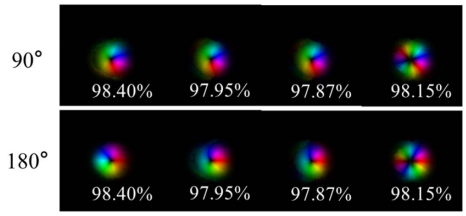

Fig. 10. Test results of four input states with different phase rotation angles.

Table 2. Test Results of Four Input States under the Influence of Different Turbulences

C_n^2 (10^{-16} $m^{-2/3}$)	00	01	10	11
1	98.18%	96.75%	96.24%	97.23%
5	97.58%	86.11%	92.53%	90.57%
10	96.46%	90.26%	83.04%	81.59%
50	78.72%	75.37%	71.88%	74.37%
100	77.74%	66.98%	64.21%	68.04%
150	59.07%	69.55%	49.48%	45.30%

(a)

B \ A	-1	0	1
-1	-1	-1	-1
0	-1	0	0
1	-1	0	1

(b)

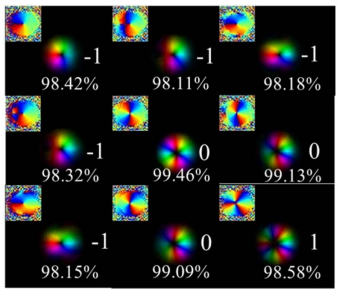

Fig. 11. Balanced ternary logic AND operation with OAM modes. (a) Truth table. (b) Results predicted by the 5-layer ODNN.

trained with 8000 iterations, which took approximately 40 min, the ODNN accurately implemented the AND operation for all input data. As shown in Fig. 11(b), although the intensity distribution of some output light fields is distorted, it does not affect the performance of the logical gate with mode dimension as the logic judgment state because the phase and mode information are well modulated with mode purities exceeding 98%. Similarly, the other six basic logical operations can also be implemented. This demonstrates that the proposed logic calculation method based on the OAM mode can realize higher-ary logical operations and provides an effective method for optical digital computing with high parallel processing capabilities.

4. CONCLUSIONS

In summary, we proposed and investigated an OAM logical operation using ODNNs. OAM logic states have a natural strong distinction, certain robustness, and infinite division space, which provide the possibility for multi-ary logical operations. To complete the independent mode and spatial position modulation of multiple light fields required in OAM logic, we designed an ODNN framework that combines optical diffraction and deep learning to solve the multi-plane diffractive structure by directly updating the phase and amplitude distributions. The simulation results show that the proposed ODNN model can automatically solve the linear system response of the multi-light field and can accurately perform logic AND, OR, NOT, NAND, and NOR operations. This nondestructive optical operation on the physical structure of the light fields significantly improves the applicability and flexible embeddability of OAM-based logics, enabling it to successfully obtain the logic XNOR and XOR gates by cascading basic logic gates. In addition, we discussed and explored the realization of OAM mode-based logic half-adder and high-ary logic gates. It is anticipated that the revealed design strategy of logic has the potential to promote the development of optical digital computing with high parallel processing ability.

5. METHODS

Combining deep learning technology [58–62] and the multi-plane diffraction structure in which the signal transmission follows the scalar diffraction theory, ODNN has both the learning ability possessed by traditional electric neural networks and the light field modulation ability. The ODNN also contains an input layer, multiple hidden layers, and an output layer, where the hidden layers are formed by the diffractive layers. Based on the Rayleigh-Sommerfeld diffraction, each diffractive unit/neuron is regarded as a secondary source and fully connected to the next layer. In the forward-propagation model of the ODNN, the propagation and superposition of secondary wave sources between two layers obey the following:

$$w^L(f_x, f_y) = \exp\left(\frac{j2\pi d_{L-1}}{\lambda}\right) \cdot \exp[-j\pi\lambda d_{L-1}(f_x^2 + f_y^2)], \tag{2}$$

where (f_x, f_y) represents the spatial frequency of (x, y) in the Lth hidden layer, and d_{L-1} is the distance from the $(L-1)$th layer to the Lth layer. j is the imaginary unit and λ is the working wavelength. The input of the $(L+1)$th layer, that is, the output of the Lth layer, can be expressed as

$$Y^L = F^{-1}[F(U^L) \cdot w^L], \tag{3}$$

where F and F^{-1} represent the Fourier transform and inverse Fourier transform, respectively. U^L is determined by the Hadamard product of the transmission coefficient t^L and the input wave, that is, $U_i^L(x, y, z) = t_i^L(x_i, y_i, z_i) \cdot Y^{L-1}(x_i, y_i, z_i)$, where i represents the neuron located at (x_i, y_i, z_i) in the Lth hidden layer. The transmission coefficient t^L satisfies $t_i^L(x_i, y_i, z_i) = a_i^L(x_i, y_i, z_i)\exp[j\phi_i^L(x_i, y_i, z_i)]$, where the amplitude and phase modulation factors are constrained by $0 \le |a_i^k| \le 1$ and $0 \le |\phi_i^k| \le 2\pi$, respectively. As a modulation method with learning ability, the ODNN manipulates the wavefront of the input beams by continuously updating neurons, and both the amplitude and phase parameters contained in each neuron can be adjusted. Here, we update the amplitude and phase values simultaneously to complete the complex wavefront modulation.

To evaluate the performance of the ODNN, we define a loss function to calculate the difference between the predicted output E and the ground truth target Y, which can be expressed as

$$L = \sum_i^N |E_i - Y_i|^2, \tag{4}$$

where N represents the pixel number of the diffractive layers, which is set to 256×256, and the size of the layers is 30 mm × 30 mm. The distance d between the two layers was 30 mm. With the forward propagation model following the optical scalar diffraction theory and the backward propagation model aimed at minimizing the loss function, the constructed ODNN can accurately solve the multi-plane system response for the target modulation and obtain the optimal structure of the diffractive layers.

The ODNN was constructed and trained using Python version 3.5.0 and Google TensorFlow version 2.3.0, with a graphics processing unit, Intel Core i9-10900k. The learning rate was set to 0.005. It took approximately 20 min to train a 4-layer ODNN with 8000 iterations.

Funding. National Natural Science Foundation of China (12047539, 61805149, 62101334); Guangdong Basic and Applied Basic Research Foundation (2019A1515111153, 2020A1515011392, 2020A1515110572, 2021A1515011762);

Shenzhen Fundamental Research Program (JCYJ20180507182035270, JCYJ20200109144001800); Science and Technology Project of Shenzhen (GJHZ20180928160407303); Shenzhen Universities Stabilization Support Program (SZWD2021013); Shenzhen Excellent Scientific and Technological Innovative Talent Training Program (RCBS20200714114818094); China Postdoctoral Science Foundation (2020M682867).

Acknowledgment. P. W. and S. C. conceived the idea of this research. P. W. and W. X. performed the simulations and built a neural network model. P. W. wrote the paper. W. X. and Z. H. provided assistance with optical diffractive neural network models. Y. H., Z. X., J. M., and S. C. shared their insights and contributed to discussions on the results. H. Y., Y. L., D. F., and S. C. supervised the project.

Disclosures. The authors declare no competing financial interests.

Data Availability. Data underlying the results presented in this paper are not publicly available at this time but may be obtained from the authors upon reasonable request.

REFERENCES

1. J. Touch, A.-H. Badawy, and V. J. Sorger, "Optical computing," Nanophotonics **6**, 503–505 (2017).
2. A. A. Sawchuk and T. C. Strand, "Digital optical computing," Proc. IEEE **72**, 758–779 (1984).
3. H. J. Caulfield and S. Dolev, "Why future supercomputing requires optics," Nat. Photonics **4**, 261–263 (2010).
4. N. D. Lane, S. Bhattacharya, A. Mathur, P. Georgiev, C. Forlivesi, and F. Kawsar, "Squeezing deep learning into mobile and embedded devices," IEEE Pervasive Comput. **16**, 82–88 (2017).
5. Z. Gu, Y. Gao, and X. Liu, "Optronic convolutional neural networks of multi-layers with different functions executed in optics for image classification," Opt. Express **29**, 5877–5889 (2021).
6. D. R. Solli and B. Jalali, "Analog optical computing," Nat. Photonics **9**, 704–706 (2015).
7. D. Xu, S. He, J. Zhou, S. Chen, S. Wen, and H. Luo, "Optical analog computing of two-dimensional spatial differentiation based on the Brewster effect," Opt. Lett. **45**, 6867–6870 (2020).
8. H. Rajabalipanah, A. Abdolali, S. Iqbal, L. Zhang, and T. J. Cui, "Analog signal processing through space-time digital metasurfaces," Nanophotonics **10**, 1753–1764 (2021).
9. D. Woods and T. J. Naughton, "Optical computing," Appl. Math. Comput. **215**, 1417–1430 (2009).
10. L. Allen, M. W. Beijersbergen, R. J. C. Spreeuw, and J. P. Woerdman, "Orbital angular momentum of light and the transformation of Laguerre-Gaussian laser modes," Phys. Rev. A **45**, 8185–8189 (1992).
11. L. Allen, S. M. Barnett, and M. J. Padgett, *Optical Angular Momentum* (CRC Press, 2016).
12. N. Bozinovic, Y. Yue, Y. Ren, M. Tur, P. Kristensen, H. Huang, A. E. Willner, and S. Ramachandran, "Terabit-scale orbital angular momentum mode division multiplexing in fibers," Science **340**, 1545–1548 (2013).
13. J. Wang, J. Y. Yang, I. M. Fazal, N. Ahmed, Y. Yan, H. Huang, Y. Ren, Y. Yue, S. Dolinar, and M. Tur, "Terabit free-space data transmission employing orbital angular momentum multiplexing," Nat. Photonics **6**, 488–496 (2012).
14. Y. He, P. Wang, C. Wang, J. Liu, H. Ye, X. Zhou, Y. Li, S. Chen, X. Zhang, and D. Fan, "All-optical signal processing in structured light multiplexing with dielectric meta-optics," ACS Photon. **7**, 135–146 (2020).
15. J. Liu, P. Wang, X. Zhang, Y. He, X. Zhou, H. Ye, Y. Li, S. Xu, S. Chen, and D. Fan, "Deep learning based atmospheric turbulence compensation for orbital angular momentum beam distortion and communication," Opt. Express **27**, 16671–16688 (2019).
16. D. G. Grier, "A revolution in optical manipulation," Nature **424**, 810–816 (2003).
17. A. E. Willner, L. Li, G. Xie, Y. Ren, H. Huang, Y. Yue, N. Ahmed, M. J. Willner, A. J. Willner, Y. Yan, Z. Zhao, Z. Wang, C. Liu, M. Tur, and S. Ashrafi, "Orbital-angular-momentum-based reconfigurable optical switching and routing," Photon. Res. **4**, B5–B8 (2016).
18. Z. Xie, S. Gao, T. Lei, S. Feng, Y. Zhang, F. Li, J. Zhang, Z. Li, and X. Yuan, "Integrated (de)multiplexer for orbital angular momentum fiber communication," Photon. Res. **6**, 743–749 (2018).
19. W. Xiong, P. Wang, M. Cheng, J. Liu, Y. He, X. Zhou, J. Xiao, Y. Li, S. Chen, and D. Fan, "Convolutional neural network based atmospheric turbulence compensation for optical orbital angular momentum multiplexing," J. Lightwave Technol. **38**, 1712–1721 (2020).
20. X. Fang, H. Ren, and M. Gu, "Orbital angular momentum holography for high-security encryption," Nat. Photonics **14**, 102–108 (2020).
21. Q. Xiao, Q. Ma, T. Yan, L. Wu, C. Liu, Z. Wang, X. Wan, Q. Cheng, and T. Cui, "Orbital-angular-momentum-encrypted holography based on coding information metasurface," Adv. Opt. Mater. **9**, 2002155 (2021).
22. S. Fu, T. Wang, and C. Gao, "Perfect optical vortex array with controllable diffraction order and topological charge," J. Opt. Soc. Am. A **33**, 1836–1842 (2016).
23. C. Huang, C. Zhang, S. Xiao, Y. Wang, Y. Fan, Y. Liu, N. Zhang, G. Qu, H. Ji, J. Han, L. Ge, Y. Kivshar, and Q. Song, "Ultrafast control of vortex microlasers," Science **367**, 1018–1021 (2020).
24. S. Fu and C. Gao, "Influences of atmospheric turbulence effects on the orbital angular momentum spectra of vortex beams," Photon. Res. **4**, B1–B4 (2016).
25. H. Wei, Z. Wang, X. Tian, M. Käll, and H. Xu, "Cascaded logic gates in nanophotonic plasmon networks," Nat. Commun. **2**, 1–5 (2011).
26. Y. Sang, X. Wu, S. S. Raja, C. Y. Wang, H. Li, Y. Ding, D. Liu, J. Zhou, H. Ahn, and S. Gwo, "Broadband multifunctional plasmonic logic gates," Adv. Opt. Mater. **6**, 1701368 (2018).
27. H. Liu, Z. Quan, Y. Cheng, S. Deng, and L. Yuan, "Ultra-compact universal linear-optical logic gate based on single rectangle plasmonic slot nanoantenna," Plasmonics **16**, 1–8 (2021).
28. A. Pal, M. Z. Ahmed, and S. Swarnakar, "An optimized design of all-optical XOR, OR, and NOT gates using plasmonic waveguide," Opt. Quantum Electron. **53**, 84 (2021).
29. Q. Xu and M. Lipson, "All-optical logic based on silicon micro-ring resonators," Opt. Express **15**, 924–929 (2007).
30. M. W. McCutcheon, G. W. Rieger, J. F. Young, D. Dalacu, P. J. Poole, and R. L. Williams, "All-optical conditional logic with a nonlinear photonic crystal nanocavity," Appl. Phys. Lett. **95**, 221102 (2009).
31. Y. Fu, X. Hu, C. Lu, S. Yue, H. Yang, and Q. Gong, "All-optical logic gates based on nanoscale plasmonic slot waveguides," Nano Lett. **12**, 5784–5790 (2012).
32. N. K. Fontaine, R. Ryf, H. Chen, D. T. Neilson, K. Kim, and J. Carpenter, "Laguerre-Gaussian mode sorter," Nat. Commun. **10**, 1865 (2019).
33. G. Labroille, B. Denolle, P. Jian, P. Genevaux, N. Treps, and J.-F. Morizur, "Efficient and mode selective spatial mode multiplexer based on multi-plane light conversion," Opt. Express **22**, 15599–15607 (2014).
34. Y. Sakamaki, T. Saida, T. Hashimoto, and H. Takahashi, "New optical waveguide design based on wavefront matching method," J. Lightwave Technol. **25**, 3511–3518 (2007).
35. F. Brandt, M. Hiekkamäki, F. Bouchard, M. Huber, and R. Fickler, "High-dimensional quantum gates using full-field spatial modes of photons," Optica **7**, 98–107 (2020).
36. X. Lin, Y. Rivenson, N. T. Yardimci, M. Veli, Y. Luo, M. Jarrahi, and A. Ozcan, "All-optical machine learning using diffractive deep neural networks," Science **361**, 1004–1008 (2018).
37. T. Yan, J. Wu, T. Zhou, H. Xie, F. Xu, J. Fan, L. Fang, X. Lin, and Q. Dai, "Fourier-space diffractive deep neural network," Phys. Rev. Lett. **123**, 023901 (2019).

38. T. Zhou, X. Lin, J. Wu, Y. Chen, H. Xie, Y. Li, J. Fan, H. Wu, L. Fang, and Q. Dai, "Large-scale neuromorphic optoelectronic computing with a reconfigurable diffractive processing unit," Nat. Photonics **15**, 367–373 (2021).
39. M. Veli, D. Mengu, N. T. Yardimci, Y. Luo, J. Li, Y. Rivenson, M. Jarrahi, and A. Ozcan, "Terahertz pulse shaping using diffractive surfaces," Nat. Commun. **12**, 37 (2021).
40. J. Shi, D. Wei, C. Hu, M. Chen, K. Liu, J. Luo, and X. Zhang, "Robust light beam diffractive shaping based on a kind of compact all-optical neural network," Opt. Express **29**, 7084–7099 (2021).
41. Z. Huang, P. Wang, J. Liu, W. Xiong, Y. He, J. Xiao, H. Ye, Y. Li, S. Chen, and D. Fan, "All-optical signal processing of vortex beams with diffractive deep neural networks," Phys. Rev. Appl. **15**, 014037 (2021).
42. A. M. Yao and M. J. Padgett, "Orbital angular momentum: origins, behavior and applications," Adv. Opt. Photon. **3**, 161–204 (2011).
43. L. Jing, X. Lin, Z. Wang, I. Kaminer, H. Hu, E. Li, Y. Liu, M. Chen, B. Zhang, and H. Chen, "Polarization shaping of free-electron radiation by gradient bianisotropic metasurfaces," Laser Photon. Rev. **15**, 2000426 (2021).
44. H. Lu, B. Zheng, T. Cai, C. Qian, Y. Yang, Z. Wang, and H. Chen, "Frequency-controlled focusing using achromatic metasurface," Adv. Opt. Mater. **9**, 2001311 (2021).
45. P. Xu, H. Tian, W. Jiang, Z. Chen, T. Cao, C. Qiu, and T. Cui, "Phase and polarization modulations using radiation-type metasurfaces," Adv. Opt. Mater. **9**, 2100159 (2021).
46. Y. He, Z. Xie, B. Yang, X. Chen, J. Liu, H. Ye, X. Zhou, Y. Li, S. Chen, and D. Fan, "Controllable photonic spin Hall effect with phase function construction," Photon. Res. **8**, 963–971 (2020).
47. Z. Ji, W. Liu, S. Krylyuk, X. Fan, Z. Zhang, A. Pan, L. Feng, A. Davydov, and R. Agarwal, "Photocurrent detection of the orbital angular momentum of light," Science **368**, 763–767 (2020).
48. E. Goi, X. Chen, Q. Zhang, B. P. Cumming, S. Schoenhardt, H. Luan, and M. Gu, "Nanoprinted high-neuron-density optical linear perceptrons performing near-infrared inference on a CMOS chip," Light Sci. Appl. **10**, 40 (2021).
49. H. Chen, J. Feng, M. Jiang, Y. Wang, J. Lin, J. Tan, and P. Jin, "Diffractive deep neural networks at visible wavelengths," Engineering, https://doi.org/10.1016/j.eng.2020.07.032 (2021).
50. M. Soskin, V. Gorshkov, M. Vasnetsov, J. Malos, and N. Heckenberg, "Topological charge and angular momentum of light beams carrying optical vortices," Phys. Rev. A **56**, 4064–4075 (1997).
51. L. Chen, W. Zhang, Q. Lu, and X. Lin, "Making and identifying optical superpositions of high orbital angular momenta," Phys. Rev. A **88**, 053831 (2013).
52. H. Sztul and R. Alfano, "Double-slit interference with Laguerre-Gaussian beams," Opt. Lett. **31**, 999–1001 (2006).
53. J. Hickmann, E. Fonseca, W. Soares, and S. Chávez-Cerda, "Unveiling a truncated optical lattice associated with a triangular aperture using light's orbital angular momentum," Phys. Rev. Lett. **105**, 053904 (2010).
54. Y. He, J. Liu, P. Wang, W. Xiong, Y. Wu, X. Zhou, Y. Cheng, Y. Gao, Y. Li, and S. Chen, "Detecting orbital angular momentum modes of vortex beams using feed-forward neural network," J. Lightwave Technol. **37**, 5848–5855 (2019).
55. Z. Huang, P. Wang, J. Liu, W. Xiong, Y. He, X. Zhou, J. Xiao, Y. Li, S. Chen, and D. Fan, "Identification of hybrid orbital angular momentum modes with deep feedforward neural network," Results Phys. **15**, 102790 (2019).
56. Z. Liu, S. Yan, H. Liu, and X. Chen, "Superhigh-resolution recognition of optical vortex modes assisted by a deep-learning method," Phys. Rev. Lett. **123**, 183902 (2019).
57. L. C. Andrews and R. L. Phillips, *Laser Beam Propagation through Random Media* (SPIE, 2005).
58. Y. LeCun, Y. Bengio, and G. Hinton, "Deep learning," Nature **521**, 436–444 (2015).
59. J. Schmidhuber, "Deep learning in neural networks: an overview," Neural Netw. **61**, 85–117 (2015).
60. H. Ren, W. Shao, Y. Li, F. Salim, and M. Gu, "Three-dimensional vectorial holography based on machine learning inverse design," Sci. Adv. **6**, eaaz4261 (2020).
61. R. Zhu, T. Qiu, J. Wang, S. Sui, C. Hao, T. Liu, Y. Li, M. Feng, A. Zhang, and C. Qiu, "Phase-to-pattern inverse design paradigm for fast realization of functional metasurfaces via transfer learning," Nat. Commun. **12**, 1 (2021).
62. Q. Zhang, H. Yu, M. Barbiero, B. Wang, and M. Gu, "Artificial neural networks enabled by nanophotonics," Light Sci. Appl. **8**, 1 (2019).